THE DISCONTINUOUS GALERKIN METHOD FOR PARTIALLY IONIZED GAS COMPRESSIBLE FLOWS UNDER THE INFLUENCE OF ELECTROMAGNETIC FIELDS

Konstantinos T. Panourgias[1] and John A. Ekaterinaris[2]

[1]Department of Mechanical Engineering and Aeronautics
University of Patras
Rio, Achaia, Greece
e-mail: panourgias@iacm.forth.gr

[2]Aerospace Engineering
Embry-Riddle Aeronautical University
Daytona Beach, FL, USA
e-mail: ekaterij@erau.edu

Keywords: High order methods, discontinuous Galerkin, partially ionized plasma, coupling, implicit time marching methods.

Abstract: *The flow of ionized gases under the influence of electromagnetic fields is governed by the coupled system of the compressible flow equations and the full Maxwell equations. In this system, coupling of the flow with the electromagnetic field is obtained through nonlinear and stiff source terms. The high-order discontinuous Galerkin finite element method is used for the numerical solution of this system. For preserving the divergence of the magnetic and the electric vector fields constraints, the perfectly hyperbolic form of the Maxwell equations is adopted for the solution of the electromagnetic field. Implicit time marching is used for the fully coupled system to avoid wrong wave shapes and propagation speeds that are obtained when the coupling source terms are lagged in time or by using splitting iterative schemes. Numerical solutions of fully and partially ionized gas flows with this fully coupled approach showed good agreement with other numerical solutions and exact results.*

1 INTRODUCTION

Plasma is referred to as the fourth state of matter. It is an ionized gas (often at high temperature) that consists of reactive particles such as electrons, ions, and radicals. Plasma in natural state is uncommon on earth but it is created in nature (lightning), it is produced in the laboratory, in devices, and industrial processes. In space however, more than 99% of all matter is in the plasma state, therefore, significant effort was devoted in magneto hydrodynamic (MHD) research in the past. Plasmas are categorized as thermal and non-thermal plasmas. In thermal plasmas the electrons and other species (atoms, ions) obtain thermal equilibrium. For non-thermal plasmas, there is a difference in temperature of electrons and other species. In certain applications, for example in combustion and flow control, non-thermal plasmas could offer an advantage over thermal plasmas because they are capable of depositing energy only in the active plasma species relevant to the flame ignition and/or flow stabilization. For plasmas to exist matter needs to be ionized. Ionization changes the characteristics of matter, such as the response to magnetic fields, and is generally achieved with relatively high power input in the gas. Plasma is often used in flow control with high intensity magnetic fields as in the case of the increase of the shock stand-off distance [1], and with high power electric fields [2], [3] in the so called dielectric barrier discharge (DBD) flow control technique.

Under certain conditions the flow of fully ionized plasma in the presence of magnetic fields can be described by the system of MHD equations. The MHD equations can be derived by coupling the Maxwell equations with an asymptotic limit of a two-fluid (ion-electron) kinetic formulation [4], [5]. The MHD equations can also be derived in the continuous limit by coupling of the fluid dynamical equations with the Maxwell's equations through the addition of Lorentz force and work in the momentum and energy equations, respectively. The derivation of the MHD equations in the continuous limit uses the assumption that $\varepsilon_e \omega / \sigma_e \ll 1$ where ε_e is the

dielectric constant, and σ_e is the electrical conductivity. Due to the assumption $\varepsilon_e \omega / \sigma_e \ll 1$, the time variation of the electric displacement in the Maxwell equations can then be ignored and a single induction equation for the magnetic field vector is obtained for the MHD system. The complete derivation of the ideal MHD system of equations, where electrostatic forces, displacement currents, viscosity, resistivity, and heat conduction are neglected can be found in [4 – 6]. However for cases where the time variations of both electric and magnetic fields are significant (ω is not necessarily small) and/or σ_e is small (in partially ionized plasmas for example), then the unsteady compressible flow equations containing electromagnetic stress, work, and heat as source terms must be coupled with the full Maxwell equations. Furthermore, for partially ionized plasmas, the local variation of the electric charges (i.e. concentration of electrons) leads to considerable electric displacements and hence, the full Maxwell equations must be used. A complete derivation of these equations is given in [7], [8].

The system of the N-S/ full Maxwell equations is coupled through the source terms. This fully coupled system constitutes a multi-scale problem where the time scales of the flow are determined by the flow speed and turnaround time of eddies and the timescales of the electromagnetic field are imposed by the speed of light. Therefore, this problem could become stiff because of the rather different time scales. Implicit time marching schemes based on the Jacobian-free Newton–Krylov (JFNK) method [9], [10] can be used to overcome the time-step limitation introduced by any explicit scheme. A way to advance this coupled system in time is to solve separately the flow equations and the Maxwell equations by lagging the source terms. However, it was found that this approach yields incorrect propagation speeds and strengths of waves. Therefore, a fully coupled monolithic approach is adopted, advancing simultaneously both systems of equations.

The discontinuous Galerkin (DG) method [11 – 15] is used for the space discretization of the fully coupled system of equations. DG as a high order accurate finite element method is well suited for the solution of ionized flows with strong discontinuities embedded in smooth but complex flow features. The DG method has good discontinuity capturing capabilities and as it will be shown in the results section discontinuities in plasma occur both in flow quantities and the electromagnetic field. It is also well suited for application of h- and p-type adaptive refinement strategies and parallel implementation. Mixed-type elements can be also readily used if the complexity of the geometry requires use of unstructured meshes without any lack of accuracy of the solution. Implementation for mixed-type unstructured meshes is facilitated with the general framework of collapsed coordinate systems [16] introducing the computational space where all numerical operations are carried out.

2 GOVERNING EQUATIONS

The set of equations that describes the motion of fully ionized gases, assuming that the charge density is everywhere zero and adopting the one-fluid concept, under the influence of arbitrary electromagnetic fields consists of the Navier-Stokes (N-S) equations augmented by a body force source term ($\mathbf{j}\times\mathbf{B}$) in the momentum equations and an electromagnetic energy source term ($E_{em} = \mathbf{E}\cdot\mathbf{j}$) in the energy equation, and the full set of the Maxwell equations for the electric and magnetic field vectors. For a Cartesian coordinate system, this set of coupled equations can be written in conservation law form:

$$\frac{\partial \mathbf{U}}{\partial t} + \frac{\partial \mathbf{F}}{\partial x} + \frac{\partial \mathbf{G}}{\partial y} + \frac{\partial \mathbf{H}}{\partial z} = \mathbf{S} \tag{1}$$

where $\mathbf{U} = [\mathbf{U}_f, \mathbf{U}_e]^T = [(\rho, \rho\mathbf{v}, \rho e), (\mathbf{B}, \mathbf{E})]^T$ is the state variable vector containing the conservative flow variables vector $\mathbf{U}_f$, and the electromagnetic field variables vector $\mathbf{U}_e$, including the electric field vector, $\mathbf{E}$ (also called electric field intensity), and the magnetic vector $\mathbf{B}$ (also called magnetic field density or magnetic flux density). The flux vectors **F**, **G** and **H** contain fluxes of the N-S and the Maxwell system. The source vector **S** which essentially couples the fluid motion with the electromagnetic field, contains nonlinear terms as products of flow and electromagnetic field variables. The set of the full Maxwell equations the Faraday law of induction and the Ampere's law for the electric field with Maxwell's corrections, are:

$$\begin{aligned} \frac{\partial \mathbf{B}}{\partial t} &= -\nabla\times\mathbf{E} \\ \frac{\partial \mathbf{E}}{\partial t} &= \frac{1}{\varepsilon_e}\left(\frac{\nabla\times\mathbf{B}}{\mu_e} - \mathbf{j}\right) \end{aligned} \tag{2}$$

Subject to the following implicit constraints for the electric field intensity **E** and the magnetic flux density **B** vectors:

$$\nabla \cdot \mathbf{E} = \frac{\rho_c}{\varepsilon_e}, \quad \nabla \cdot \mathbf{B} = 0 \tag{3}$$

In eqs (2) and (3), $\mu_e = 4\pi \times 10^{-7}\ kg\,m/(Coulomb)^2$ is the magnetic permeability of free space also called magnetic constant, $\varepsilon_e = 8.845 \times 10^{-12}\left(Coulomb\right)^2 s^2/kg\,m^3$ is the permittivity of free space or dielectric constant, and ρ_c is the total charge density including both free and bound charges. The term $1/\varepsilon_e\mu_e$ in eqn (2) is the square of the speed of light $c_e = \sqrt{1/\varepsilon_e\mu_e} = 2.998 \times 10^8\ m/s$. The term, $\mathbf{j}$ in eqn (2), is the current density that is the sum ($\mathbf{j} = \rho_c\mathbf{v} + \mathbf{J}$) of the convection and conduction current. The conduction current is given by the following relation:

$$\mathbf{J} = \sigma_e\left(\mathbf{E} + \mathbf{v} \times \mathbf{B}\right) \tag{4}$$

where σ_e is the conductivity that for fully ionized plasmas has large value and can be considered uniform and constant in space.

• • satisfy the magnetic and the electric divergence condition two new scalar variables φ and ψ are introduced, which transform the elliptic type Gauss' equations into two purely hyperbolic equations as:

$$\frac{1}{\chi}\frac{\partial \varphi}{\partial t} + \nabla \cdot \mathbf{E} = \frac{\rho_c}{\varepsilon_e}, \quad \frac{1}{c^2\gamma}\frac{\partial \psi}{\partial t} + \nabla \cdot \mathbf{B} = 0 \tag{5}$$

where χ and γ are Langrange-multiplier-like scalar coefficients and for $\chi, \gamma \to \infty$ the divergence conditions (eqn (3)) are satisfied exactly. Once the scalar variables χ and γ are introduced, the complete set of equations that must be solved in order to obtain the electromagnetic field numerical solution, satisfying, at the same time, the divergence conditions at a small tolerance, are known as perfectly hyperbolic Maxwell's equations (PHM) [17], [18], [19]:

$$\begin{aligned}
&\frac{\partial \mathbf{B}}{\partial t} + \nabla \times \mathbf{E} + \gamma \nabla \psi = 0 \\
&\frac{1}{c^2}\frac{\partial \mathbf{E}}{\partial t} - \nabla \times \mathbf{B} + \chi \nabla \varphi = \mu_e \mathbf{j} \\
&\frac{1}{\chi}\frac{\partial \varphi}{\partial t} + \nabla \cdot \mathbf{E} = \frac{\rho_c}{\varepsilon_e} \\
&\frac{1}{c^2\gamma}\frac{\partial \psi}{\partial t} + \nabla \cdot \mathbf{B} = 0
\end{aligned} \tag{6}$$

The Ampere's and Faraday's law is coupled with the two new hyperbolic equations through the terms $\gamma\nabla\psi$, $\chi\nabla\varphi$ which constitutes the correction of the electromagnetic variables in order for the divergence conditions to be enforced. Thus, the φ and ψ are called "correction potentials" and the coefficients χ and γ denote the error propagation speeds.

In the case of two-temperature partially ionized gas flows, the three species (electrons, positive ions and neutral particles) approach is adopted for a monoatomic gas. The same form of equations described above is used with the exception that two additional continuity equations for the electrons and the positive ions and one more energy equation for the electrons are solved. Therefore, for partially ionized gas flows the solution vector become $\mathbf{U} = [\mathbf{U}_f, \mathbf{U}_e]^T = [(\rho_e, \rho_i, \rho, \rho\mathbf{v}, \rho e, \rho_e e_e), (\mathbf{B}, \mathbf{E})]^T$ where ρ_e, ρ_i is the density of electrons and ions, respectively and $\rho_e e_e$ is the total energy of electrons which in general have different than the heavy particles

temperature. In this case, the total current density in eqn (4) is computed in a different way without using the electrical conductivity as follows:

$$\mathbf{j} = \sum_{i=1}^{3} (q_i n_i \mathbf{v} + q_i n_i \mathbf{U}_i) = \rho_c \mathbf{v} + \mathbf{J} \tag{7}$$

where $\mathbf{U}_i$ is the diffusion velocity of the (i) species with regard to the mixture, n_i is the density number and q_i is the charge of one particle of the species (i). The diffusion velocities $\mathbf{U}_i$ are obtained from Boltzmann's equation with the Chapman-Enskog collision integral:

$$\vec{U}_i = \frac{n_t}{n_i \rho k T_i} \sum_{s=1}^{N} m_s \left(D_{is} d_s + D_{is}^{\theta} \beta_s \vec{\nabla} \ln \theta \right) - \frac{D_i^T}{n_i m_i} \vec{\nabla} \ln T_h - \frac{D_i^{\theta *}}{n_i m_i} \vec{\nabla} \ln \theta \tag{8}$$

where T_i and m_i is the temperature and the mass of particles of (i) species, $\theta = T_e / T_h$, $D_{is}, D_i^T, D_{is}^{\theta}, D_{is}^{\theta *}$ are diffusion coefficients, $\beta_s = -w_s w_e p / D$ and $D = 1 + w_e(\theta - 1)$. A complete derivation of the term d_i that contains the driving forces is given in [20].

3 NUMERICAL APPROACH

The numerical solution of the coupled equations (see eqn (1)) describing the motion of fully ionized gas (plasma) under the influence of electromagnetic fields is obtained with the discontinuous Galerkin (DG) finite element method [12 – 15]. Multiplying the eqn (1) by a weighting function, w_i, integrating over the element K, and replacing the volume integrals involving divergence using the Gauss' theorem, the weak form of the equations is obtained:

$$\int_K w_i \frac{\partial \boldsymbol{U}}{\partial t} dK = \int_K \nabla w_i \cdot \boldsymbol{Q}(\boldsymbol{U}, \nabla \boldsymbol{U})\, dK - \int_{S_K} w_i \boldsymbol{Q}(\boldsymbol{U}, \nabla \boldsymbol{U}) \cdot \boldsymbol{n}\, dS_K + \int_K w_i \cdot \boldsymbol{S}(\boldsymbol{U})\, dK \tag{9}$$

where $\boldsymbol{Q} = (\boldsymbol{F}, \boldsymbol{G}, \boldsymbol{H})$ is the tensor of fluxes including at every line the fluid fluxes and the electromagnetic fluxes, *K* is the element, and $\boldsymbol{n}$ is the normal unit vector on ∂K which denotes the surface enclosing the element *K*. Assuming a set of non-overlapping finite elements E= {K} which fills the domain • , the discrete solution in each element, is approximated by a piecewise polynomial function which is discontinuous on the element faces. The DG method uses the same polynomial space for the expansion functions as the weight functions and the approximate solution $\boldsymbol{U}_h$ is defined as: $\boldsymbol{U}_h = \sum_i c_i w_i$ where the coefficients c_i are the degrees of freedom in each element to be advanced in time. The discretized weak form of eqn (9) is:

$$\mathbf{M}_e \frac{\partial \mathbf{c}}{\partial t} = \int_K \nabla w_i \cdot \boldsymbol{Q}(\boldsymbol{U}_h, \nabla \boldsymbol{U}_h)\, dK - \int_{S_K} w_i \widehat{\boldsymbol{Q}}(\boldsymbol{U}_h, \nabla \boldsymbol{U}_h) \cdot \boldsymbol{n}\, dS_K + \int_K w_i \boldsymbol{S}(\boldsymbol{U}_h)\, dK \tag{10}$$

where $\mathbf{M_e}$ denotes the mass matrix of the element and S_K are the faces of element K.

The h/p finite element framework [16] is used and hexahedral, prismatic, or tetrahedral elements of the physical space can be transformed into canonical cubical elements of the computational domain through collapsed coordinate transformations [16]. In our implementation, all these elements are supported. Orthogonal Legendre polynomial bases are chosen as expansion functions for the conservative flow variables and the electromagnetic field components. Because of the discontinuous nature of the solution between the elements, the surface integral is not uniquely defined. Suitable numerical fluxes are therefore required to impose uniqueness of fluxes and local conservation. Any suitable Riemann solver [21] may be used for the interface flux that does not

include viscous terms and it is simply $\widehat{\boldsymbol{Q}}(\boldsymbol{U}_h)\cdot\mathbf{n}$. For the discretization of the diffusive terms of the N-S equations, the gradient $\nabla\boldsymbol{U}_h=\boldsymbol{\Theta}$ (mixed type formulation of N-S equations) is computed first and then the LDG method [22] is used for the flux $\widehat{\boldsymbol{Q}}(\boldsymbol{U}_h,\nabla\boldsymbol{U}_h)$. For the convective fluxes, Local-Lax-Friedrichs (LLF) flux is used.

Although DG method can be advanced using explicit time marching schemes the speed of light in the Maxwell equations would impose severe CFL stability limitations. As a result, implicit time marching is chosen for the Maxwell equations in order to enable advancement the Maxwell equations simultaneously with NS equations on a collocated mesh discretization. The time advancement of the coupled NS/Maxwell system of equations is carried out with a second order accurate in time, diagonally implicit Runge-Kutta method (DIRK2):

$$\begin{aligned}
&\text{step 1:} \quad \mathrm{M}c^{n,1}=\mathrm{M}c^{n}+\Delta tR(t^{n,1},c^{n,1})\\
&\text{step 2:} \quad \mathrm{M}c^{n,2}=\mathrm{M}c^{n}+\Delta tR(t^{n,2},c^{n,2})-\Delta tR(t^{n,1},c^{n,1})\\
&c^{n+1}=c^{n}+0.5\Delta t\mathrm{M}^{-1}R(t^{n,1},c^{n,1})+0.5\Delta t\mathrm{M}^{-1}R(t^{n,2},c^{n,2})
\end{aligned} \tag{11}$$

Higher order implicit RK methods may be used for high order (4rd or higher) polynomial expansions. The Jacobian-free Newton Krylov method is used for the solution of each non-linear system of eqn (11). The iterative GMRES method in conjunction with a block Jacobi preconditioner is employed in order to accelerate the convergence of the solution of the linear systems.

4 RESULTS

4.1 Brio and Wu shock tube problem

The Brio and Wu shock tube problem [23] is a standard one-dimensional test case for MHD. It is a coplanar MHD Riemann problem analogous to the Sod's shock tube problem for gas dynamics with a constant magnetic field B_x added along the *x* direction and a discontinuous magnetic field B_y in the *y* direction. The Brio and Wu problem is solved in the domain, $-1\le x\le 1$, The initial conditions for the left and right states are:

$$\begin{aligned}
U_L&=\left[\rho_L,\,u_L,\,\upsilon_L,\,p_L,\,(B_x)_L,\,(B_y)_L,\,(E_z)_L\right]=\left[\quad 1,\,0,\,0,\,1.0,\,0.75,\,+1.0,\,0\ \right]\quad -1\le x<0\\
U_R&=\left[\rho_R,\,u_R,\,\upsilon_R,\,p_R,\,(B_x)_R,\,(B_y)_R,\,(E_z)_R\right]=\left[0.125,\,0,\,0,\,0.1,\,0.75,\,-1.0,\,0\ \right]\quad 0\le x\le 1
\end{aligned} \tag{12}$$

The specific heats ratio is set to $\gamma=2$ and the solution is run until final time t=0.01. This problem encompasses the complex wave structure [25] supported by the MHD system.

The computed with P1 expansion, density ρ, pressure *p*, velocity components, and B_y are compared in Fig. 1-(a) with the numerical solution of the MHD equations obtained with the WENO-5 scheme [24]. For comparison, a numerical solution was computed by advancing implicitly but independently the flow and the Maxwell equations by lagging in time the source terms. The comparison of the numerical solution obtained with P1 expansion using fully implicit treatment of the source terms shown of Fig. 1-(a) is in good agreement with the MHD numerical solution.

A numerical solution was also obtained where the Euler equations including the source terms were first implicitly advanced in time, and then separate implicit time marching of the Maxwell equations was performed. For this segregated time advancement strategy, the source terms that essentially couple the system cannot be advanced simultaneously and must be taken from the previous time step. This lag of the source terms in time however appears to cause significant accumulation of phase and amplitude errors and results into incorrect wave speed as it is shown in Fig. 1-(b). Similar trends were observed for other time dependent plasma flows and it was therefore concluded that there are compelling reasons to use a fully coupled numerical approach. The results of Fig. 1-(b) clearly indicate that following the segregated time advancement approach significant discrepancies with the MHD solution are obtained. The Brio and Wu problem encompasses different wave speeds. It appears that wrong wave speeds and wave strengths are always obtained when the source terms are lagged in time.

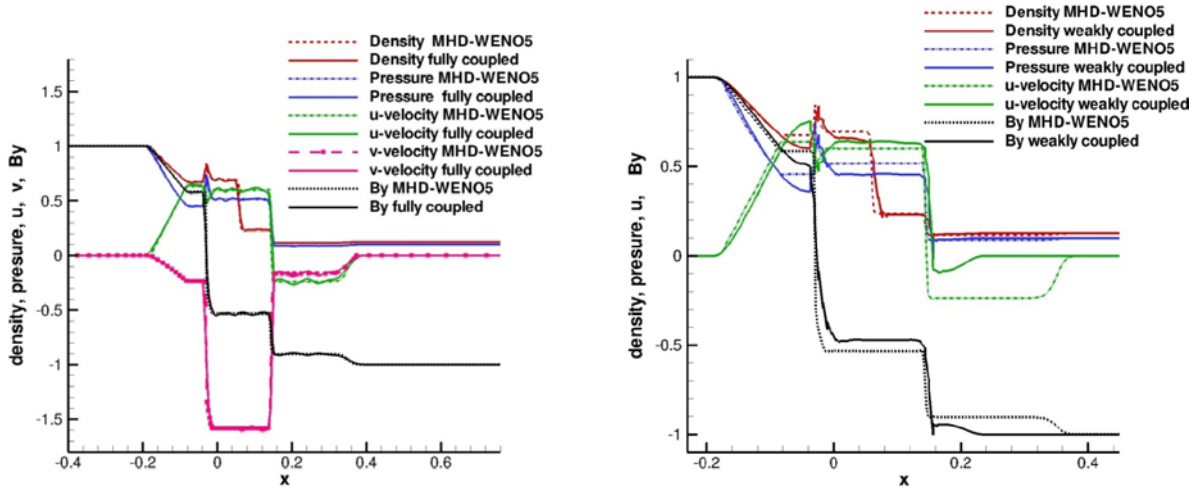

(a) (b)

Figure 1: (a) Comparison of the numerical solution obtained by the coupled method with the WENO-5 numerical solution using the MHD approximation. (b) Effect of segregated time advancement of the coupled equations; lagging in time the source terms causes wrong wave speeds and wave amplitudes.

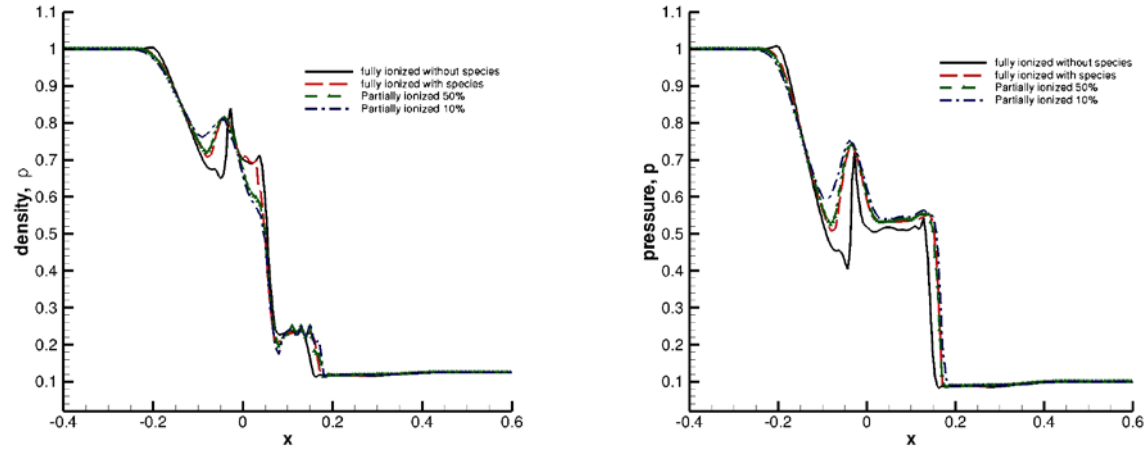

(a) (b)

Figure 2: Comparison of the (a) density and (b) pressure computed using the partially ionized gas formulation at different degrees of ionization with the solution obtained by the fully ionized formulation.

Next the Brio and Wu problem was solved using the partially ionized gas formulation with certain degrees of ionization. In Fig. 2-(a) and 2-(b), the density and the pressure, respectively, solved with 10%, 50% and 100% ionization is compared with the solution obtained by the fully ionized gas formulation. It appears that as the degree of ionization increases the solution is converges to the solution of fully ionized approach. In Fig. 3-(a), the computed electrical conductivity is shown. After the solution has been obtained the electrical conductivity is computed as $\sigma_e = |\mathbf{j}| / |\mathbf{E}|$. The computed diffusion velocity of the electrons is shown in Fig. 3-(b).

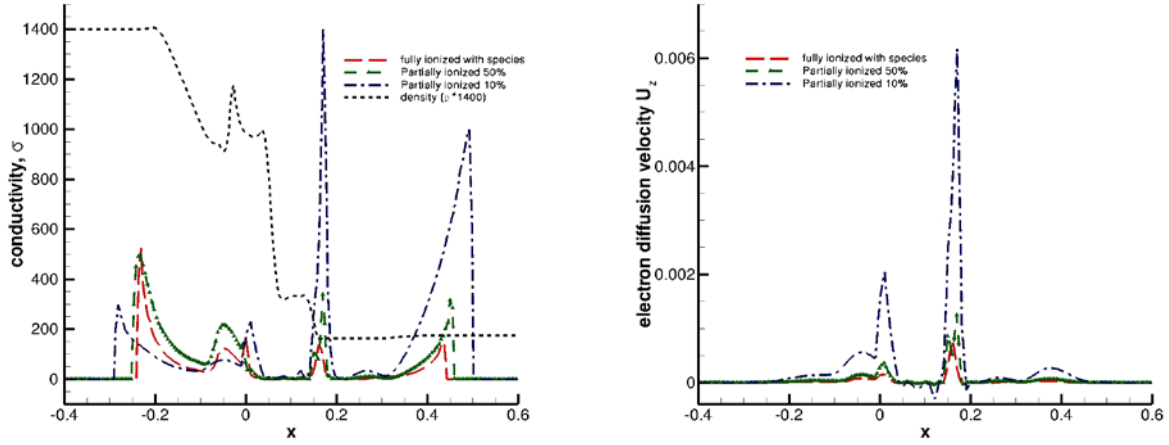

(a) (b)

Figure 3: (a) The distribution of the electrical conductivity as it is computed by the flow quantities for different degrees of ionization. (b) The diffusion velocity of electrons for different degrees of ionization.

4.2 The rotor problem

The rotor problem was introduced by Balsara [25] as a test case for demonstrating high resolving ability of numerical schemes for MHD. It is dominated by torsional Alfvén (intermediate) waves, the numerical solution of the rotor problem is very sensitive to accumulation of divergence errors (violation of the $\nabla \cdot \mathbf{B} = 0$ constraint), and the level of accuracy of the numerical method. The rotor problem was used as test case [25] [26] to verify the ability of state-of-the art numerical schemes for MHD to retain buildup of non-zero divergence to very low levels.

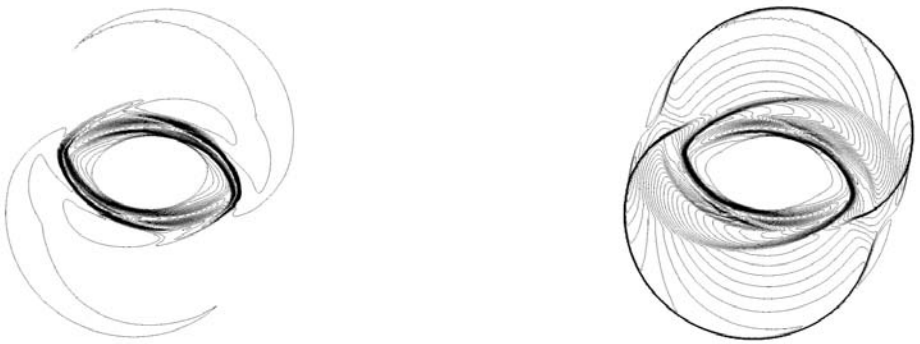

(a) density, • (b) pressure, p

Figure 4: Computed (a) density and (b) pressure at t=0.15 for the rotor problem. for comparison, 30 contour levels are used the same as Toth [23]: $0.483 < \rho < 12.95$, $0.0202 < p < 2.008$.

The rotor problem is solved numerically in the unit square $0 \le x \le 1$, $0 \le y \le 1$ using an 400×400 element mesh. The rotor is the circular region of radius 0.1 located at the center of the computational domain where the density is 10 and a toroidal velocity distribution is specified. The initial density and pressure are one everywhere else. A uniform magnetic field of five units is applied along the *x* direction in the entire domain. The numerical solution was computed with P1 expansions and it is advanced until the final time t=0.15 before any disturbances resulting from the interaction of the flow with the imposed magnetic field reached the boundaries. Therefore PML regions were not required for the numerical solution of the Maxwell equations. Contour plots of density, pressure, Mach number, and magnetic pressure are shown in Fig. 4 and 5. These were obtained from the

numerical solution of the coupled system and they are in perfect agreement with other high resolution MHD solutions [26]. In addition, the computed component of the electric filed E_z normal to the (x, y) plane along the z direction is shown in Fig. 6-(a). A contour plot of the current in the z direction $J_z/\bullet_e$ is shown in Fig. 6-(b). The percentage violation of the divergence free constraint is shown in Fig. 7-(a) and the elements where limiting was performed are marked in Fig. 7-(b). It appears that only small divergence accumulations occur mainly at the locations of discontinuities.

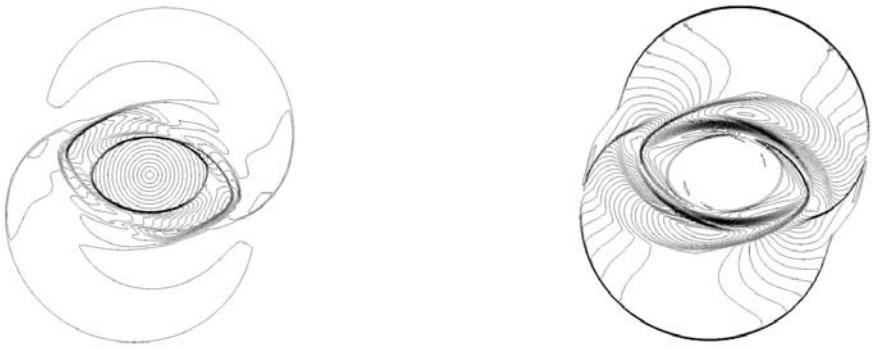

(a) Mach number, M

(b) Magnetic pressure, $|B|^2/2$

Figure 5: Computed Mach number and Magnetic pressure at t=0.15 for the rotor problem. for comparison, 30 contour levels are used the same as Toth [23]: $0 < M < 8.18$, $0.017 < |\mathbf{B}|^2/2 < 2.642$.

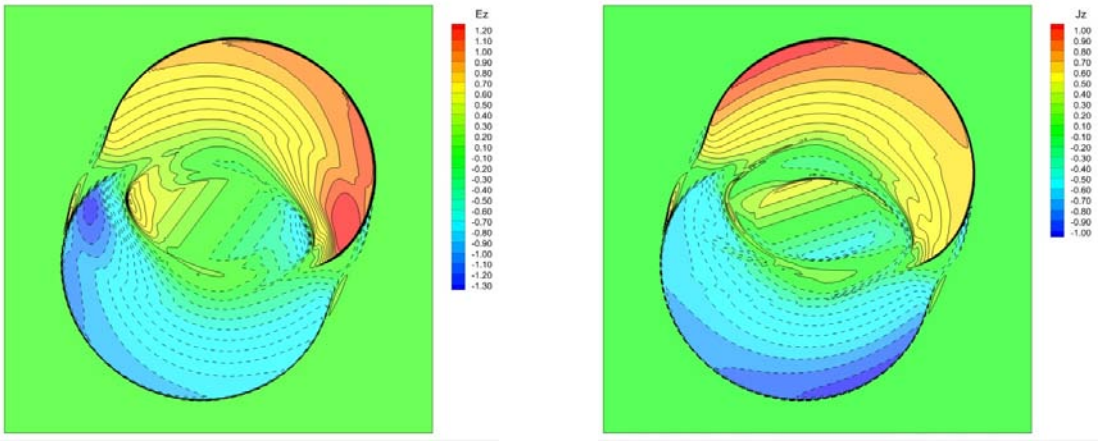

(a) electric field component Ez

(b) $J/\bullet_e$

Figure 6: (a) Computed electric field, normal to the xy plane component, E_z, (dashed lines denote negative values), (b) Current density, $J_z/\bullet$.

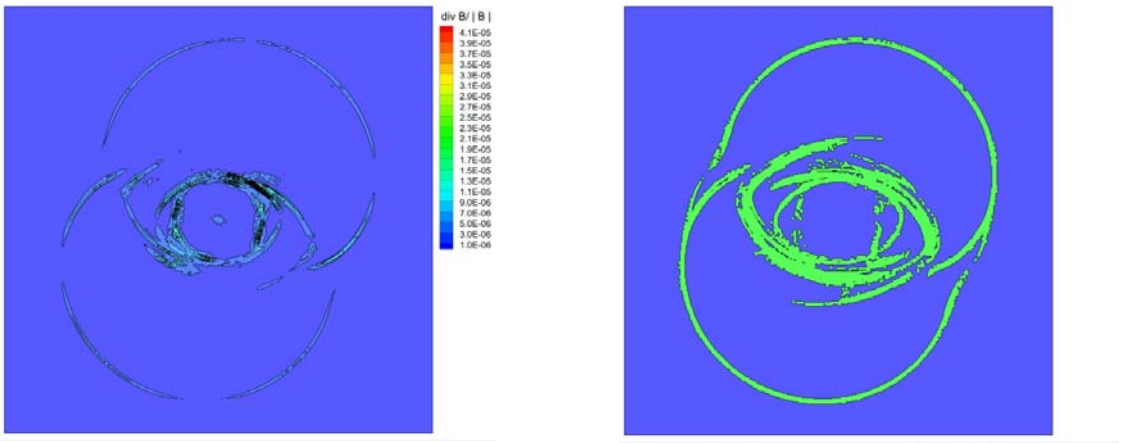

(a) **div** B (b) limited elements

Figure 7: (a) Deviation from the divergence-free constraint, (b) element where the TVB limiter was activated.

4.3 Control of shock standoff distance

The Lorentz force term opposes the motion of the ionized gas across the magnetic streamlines. As a result, a magnetic field applied on a conductive high speed ionized shock layer over a blunt body tends to increase the drag, to slow down near the surface flow, and reduce heat transfer and skin friction. An approximate analytic solution for the stagnation region of high flow over a sphere altered by a magnetic dipole field introduced at the center of the sphere was found by Bush [27], [28]. The analytical solution predicted flow deceleration that resulted in increased shock standoff distance and reduction in stagnation point heat transfer proportional to the intensity of the applied magnetic field. In aerospace applications the plasma could be partially ionized. As it has been noted before, computation of partially ionized plasma flows requires numerical solution of additional equations for the conservation of species. We considered fully ionized plasma with uniform conductivity flowing over a sphere that is composed from non-conducting and non-magnetic material and imposing the same as Poggie and Gaitonde [3] cylindrically symmetric $(\vec{e_r}, \vec{e_\theta})$, magnetic dipole field: $\mathbf{B} = \frac{\cos\theta}{r^3}\vec{e_r} + \frac{\sin\theta}{2r^3}\vec{e_\theta},$ located at the center of the sphere. The magnetic field is symmetric with respect to the polar angle θ and decays with distance from the center r as $1/r^3$. We solve the coupled system of NS/Maxwell equations for the flow of fully ionized gas at Mach number M=5. A reference inviscid flow solution over the sphere at Mach 5 flow was computed without the magnetic field. For the computation with the dipole magnetic field, the domain was truncated (see Fig. 8-(a)) to the size necessary for the computation of the flow. Therefore it was necessary to use PML layers outside of the main domain where the coupled system is solved to avoid spurious numerical reflections from the Maxwell equations. The PML system is a system of 12 equations [29] similar to the Maxwell equations that is also solved implicitly in the PML domain only. The PML domains surrounding the computational domain are shown in Fig. 8-(a) and they consist of four layers outside the main domain where the coupled system is solved. The electromagnetic field was parameterized [1] with the non-dimensional quantity $Q = \sigma_e (B_{g_0})^2 R_b / \rho_\infty V_\infty$ where R_b is the radius of the sphere and B_{g_0} denotes the magnetic field intensity at the pole (stagnation point) of the sphere. A value $Q = 6$ of the non-dimensional quantity (same as in [1]) was used for the computations. The comparison of the computed flow with the magnetic field off and the magnetic field on is shown in Figs. 8-(b) and 8-(c). Clearly, the magnetic dipole resulted in an increase of the standoff shock distance shown both in the pressure distribution of Fig. 8-(b) and the Mach number distribution of Fig. 8-(c). The resulted increase of the bow shock standoff distance, Δ_s / R_b, where $\Delta_s = R_s - R_b$ and R_s is the shock location was the same with the increase obtained in [1] where the influence of both electric and magnetic fields was considered in a different formulation for steady state flows. The increase of the low speed region is demonstrated in Fig. 8-(c) and it is shown that the sonic line was significantly displaced due to the influence of the magnetic field.

Next, this problem with the same configuration is solved using the partially ionized gas formulation with 50% ionization. In Figs. 9-(a) and 9-(b) the density and the Mach number is shown, respectively. In Figs. 9-(c) and 9-(d) the computed electrical conductivity and the electrons' diffusion velocity is shown.

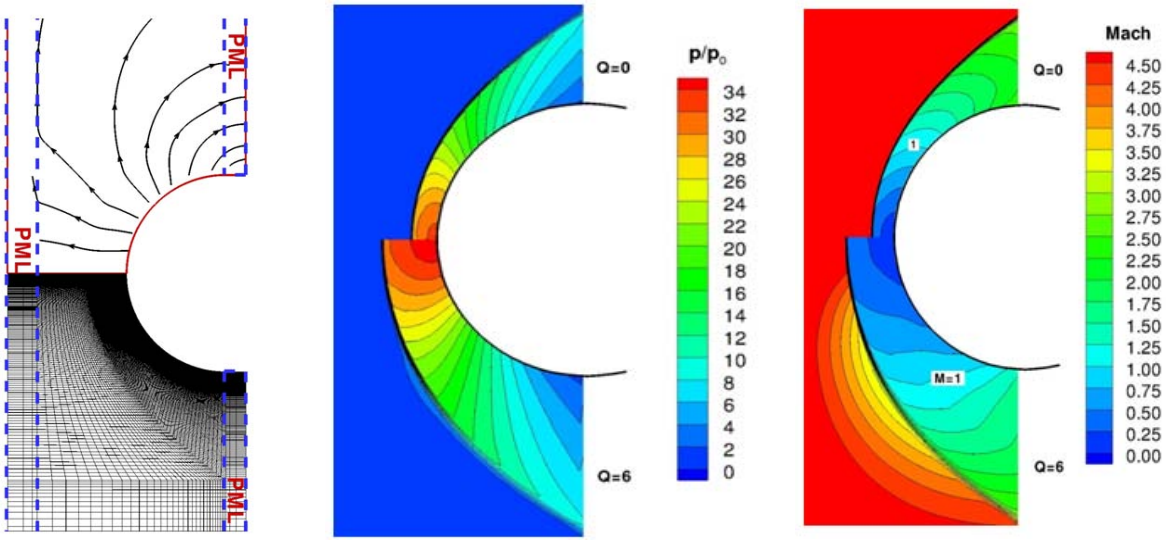

(a) (b) (c)

Figure 8: (a) Computational mesh and the surrounding PML regions. Comparison of the computed (b) pressure and (c) Mach number distribution without (Q=0) and with (Q=6) a magnetic dipole at the center.

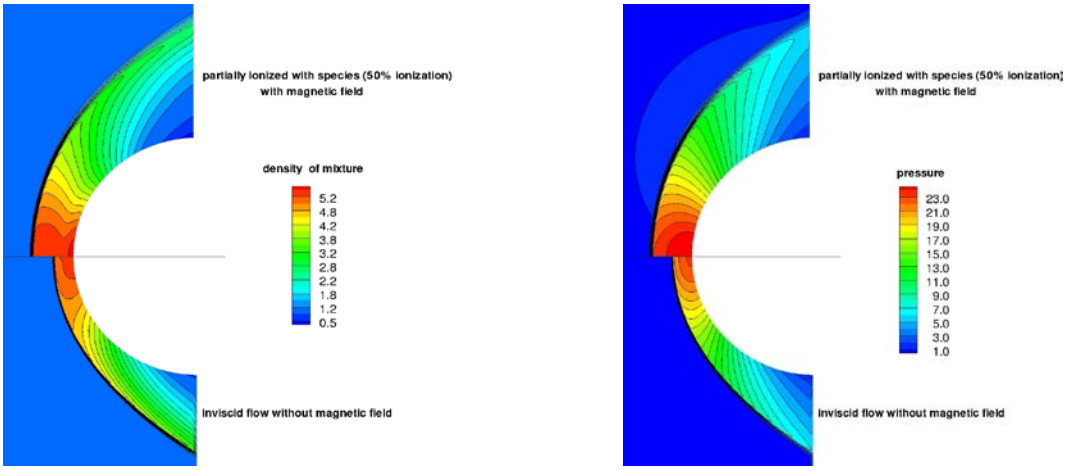

(a) (b)

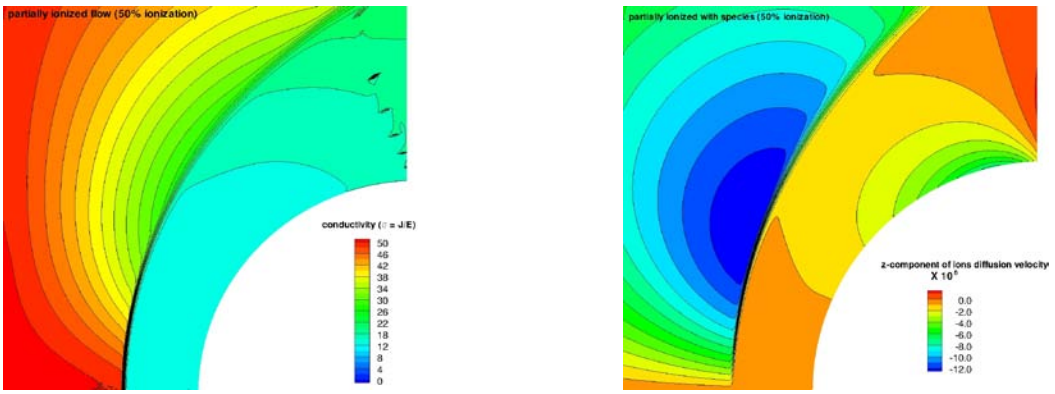

(c) (d)

Figure 9: (a) Comparison of the computed density (50% ionized gas) without and with magnetic field. (b) Comparison of the computed pressure (50% ionized gas) without and with magnetic field. (c) A close view of the computed electrical conductivity. (d) A close view of the electron's diffussion velocity.

ACKNOWLEDGEMENTS

We gratefully acknowledge financial support for this work provided by Thales project: ANEMOS - "Analytical and Numerical Electromagnetism with Applications in Photonics and Nanodevices - MIS **379522**".

REFERENCES

[1] Poggie J, Gaitonde DV. Magnetic control of flow past a blunt body: Numerical validation and exploration. *Physics of Fluids* 2002; **15**(4): 1720-1731**.**
[2] Corke TC, Post ML, and Orlov DM. SDBD plasma enhanced aerodynamics: concepts, optimization and applications. *Progress in Aerospace Sciences* 2007; **43**(7–8): 193-217.
[3] Mertz BE, Corke, TC. Single-dielectric barrier discharge plasma actuator modelling and validation. *Journal of Fluid Mechanics* 2011; **66**: 557-583.
[4] Sherclieff, J.A., *A Textbook of Magnetohydrodynamics, Pergamon Press*, New York, 1965.
[5] Landau, L.D. and Lifshits, E., *Electrodynamics of Continuous Media, Pergamon Press*, New York, 1960.
[6] Powell KG, Roe PL, Linde TJ, Gombosi TI, De Zeeuw DL. Solution-Adaptive Upwind Scheme for Ideal Magnetohydrodynamics. *Journal of Computational Phys*ics 1999; **154**(2): 284-309.
[7] Giordano D. Hypersonic Flow Governing Equations with Electromagnetic Fields. *AIAA Paper* 2002-2165, June 2002.
[8] Pai, S.I., *Magnetohydrodynamics and Plasma Dyanmics*, Springer Verlag, 1963.
[9] Knoll DA, Keyes DE. Jacobian-free Newton–Krylov methods: a survey of approaches and applications. *Journal of Computational Phys*ics 2004; **193**(2): 357-397.
[10] Brown PN, Saad Y. Hybrid Krylov Methods for Nonlinear Systems of Equations. *SIAM Journal of Scientific and Statistical Computing* 1990; **11**: 450–481.
[11] Reed WH, Hill TR. Triangular mesh methods for the neutron transport equations. Technical Report LA-UR 73-479, Los Alamos Scientific Laboratory, 1973.
[12] Cockburn B, Shu C-W, The Runge-Kutta Discontinuous Galerkin Method for Conservation Laws V: Multidimensional Systems. *Journal of Computational Phys*ics 1998; **141**(2): 199-224.
[13] Cockburn B, Shu C-W, Hou S. The Runge-Kutta local projection discontinuous Galerkin finite element method for conservation laws IV: The multi-dimensional case. *Mathematics of Computation* 1990; **54**: 545 – 581.
[14] Cockburn B, Shu, C-W. TVB Runge-Kutta Local Projection Discontinuous Galerkin Finite Element Method for Conservation Laws II: General framework. *Mathematics of Computation* 1989; **52**: 411-435.
[15] Cockburn B, Lin S-Y, Shu C-W. TVB Runge-Kutta local projection discontinuous Galerkin finite element method for conservation laws III: One-dimensional systems. *Journal of Com. Phys*ics 1989; **84**(1): 90-113.
[16] Karniadakis, GE, Sherwin SJ. Spectral/hp Element Methods for CFD. Oxford Univ. Press, 2005.
[17] C.-D. Munz, P. Omnes, R. Schneider, E. Sonnendrcker, and U. Vo, "Divergence Correction Techniques for Maxwell Solvers Based on a Hyperbolic Model," Journal of Computational Physics, vol. 161, no. 2, pp. 484–511, 2000.
[18] C.-D. Munz, P. Ommes, and R. Schneider, "A three-dimensional finite-volume solver for the Maxwell equations with divergence cleaning on unstructured meshes," Computer Physics Communications, vol. 130, no. 1-2, pp. 83–117, 2000.
[19] C. Munz, R. Schneider, and U. Voss, "A finite-volume method for the Maxwell equations in the time domain," SIAM Journal on Scientific Computing, vol. 22, no. 2, pp. 449–475, 2000.
[20] Rat, V., Andre, P. Aubreton, J., Elchinger, M.F. Fauchais P., and Lefort, A., **"**Transport properties in two-temperature plasma: theory and application**,"** Physical Review E, Vol. 64, 026409.
[21] Toro EF. Riemann Solvers and Numerical Methods for Fluid Dynamics. 2nd Edition, Springer-Verlag 1999.
[22] Cockburn B, and Shu C-W. The local discontinuous Galerkin Method for time dependent convection-diffusion systems. *SIAM Journal of Numerical Analysis* 1989;**35**: 2440-2463.
[23] Brio M, Wu CC. An upwind differencing scheme for the equations of ideal magnetohydrodynamics *Journal of Computational Phys*ics 1988; **75**(2): 400-422.
[24] Ekaterinaris JA. Application of a High Order Numerical Method for MHD Control of Shock Boundary Layer Interaction. *AIAA Journal* 2010; **48**(12): 2781-2792.
[25] Balsara, DS, Spicer, DS. A Staggered Mesh Algorithm Using Higher Order Godunov Fluxes to Ensure Solenoidal Magnetic Fields in MHD Simulations. *Journal of Computational Phys*ics **149**; (1999): 270-292.
[26] Toth G. The $\nabla \cdot \mathbf{B} = 0$ Constraint in Shock-Capturing Magnetohydrodynamics. *Journal of Computational Phys*ics 2000; **161**(2): 605-652.
[27] Bush WB. Magnetohydrodynamic-hypersonic flow past a blunt body. *Journal of Aerospace Sciences* 1958; **25**: 685-694.
[28] Bush WB. The stagnation-point boundary layer in the presence of an applied magnetic field. *Journal of Aerospace Sciences* 1961; **28**: 610-619.
[29] Berenger JP., Three-Dimensional Perfectly Matched Layer for the Absorption of Electromagnetic Waves, *Journal of Computational Phys*ics 1996; **127**(2): 363-379.